

Supplementary Information

Table of Contents

Supplementary Taxonomic Proposal	2
Supplementary Notes.....	5
Supplementary Note 1: Thermodynamic calculation of Mn(II) oxidation	5
Supplementary Note 2: Growth of Species B.....	5
Supplementary Note 3: Evaluation of FISH oligonucleotide probes for Species A and Species B. 5	
Supplementary Note 4: Evaluation of the ICP-MS method to measure oxidised and reduced pools of Mn	6
Supplementary Note 5: Evaluation of quantitative PCR probes for Species A, Species B and Bacteria.....	7
Supplementary Note 6: Ammonia as the anabolic N source for the co-culture.....	8
Supplementary Note 7: Oxygen respiration and energy conserving respiratory complexes in Species A.....	8
Supplementary Note 8: Electron balance between catabolism and anabolism in Species A.....	10
Supplementary Note 9: Stable isotope probing and nanoSIMS analysis	11
Supplementary Note 10: Carbon assimilation pathways in Species A	13
Supplementary Note 11: Unrestricted manganese oxidation calculation.....	15
Supplementary Information References.....	16

Supplementary Taxonomic Proposal

Description of “*Candidatus Manganitrophus*”, gen. nov.

Manganitrophus [man.gan.i.tro'phus]. N.L. n. manganum, manganese; N.L. Gr. n. trophos, feeder; N.L. masc. n. Manganitrophus, manganese feeder. Cells are pleomorphic, crescent shaped rods and exhibit a capacity for aerobic, chemolithoautotrophic growth using manganese carbonate as sole source of carbon and energy. Colonies have not yet been observed to form from single cells, and cells have not yet been grown in the absence of a co-enriched strain of a putative new betaproteobacterial species belonging to the genus *Ramlibacter*. Liquid cultures grown in MnCO₃ defined minimal medium generate small manganese oxide nodules or concretions to which the cells associated. Based on phylogenetic reconstructions using 16S rRNA gene and/or protein sequences, the genus affiliates within the proposed phylum *Nitrospirota* (*Nitrospirae*), is distinct from the genera comprising the classes *Nitrospira* and *Leptospirillia*, and clusters with sequences from not yet cultivated organisms typically recovered from subsurface karst environments, such as that of “*Ca. Troglgloea absoloni*”. The G+C content of the only representative, type species is 56.4 mol%. The type candidatus species of the candidatus genus is “*Ca. Manganitrophus noduliformans*”.

Description of “*Candidatus Manganitrophus noduliformans*” sp. nov.

Candidatus “Manganitrophus noduliformans” [nod.ul.i.for'mans]. L. gen. dim. n. noduli, of a little knot or nodule; L. part. adj. formans, forming; N.L. part. adj. noduliformans, nodule-forming. Cells exhibit aerobic, chemolithoautotrophic growth on manganese carbonate, utilizing the Mn(II) as sole energy source while fixing inorganic carbon via the reverse Tricarboxylic Acid Cycle. Cells form pleomorphic, crescent shaped rods, ca. 1.07 μm by 0.4 μm in dimension. Liquid cultures grown in manganese carbonate media generate manganese oxide nodules and concretions with which the cells associated. Colonies from single cells have not yet been observed to form in or on agar, or to grow in the absence of a co-enriched strain of a putative new betaproteobacterial species belonging to the genus *Ramlibacter*. By genomics, cells are predicted to be capable of motility by flagella or twitching, and of chemotaxis, but these have not yet been observed. The genome encodes LuxR and LuxI homologs often associated with acyl-homoserine lactone based quorum sensing. Growth by Mn(II) oxidation has been observed to occur a pH ranging between

5.7 and 7.4. Optimal growth occurs between 34 °C and 40 °C, with no growth observed at or above 44 °C. Cultures are pasteurized by incubation at 50 °C for 12 hours. Cells grow at NaCl concentrations equating to salinities ranging from 2 ppt to 16 ppt and are predicted by genomics to be able to make the compatible solute hydroxyectoine. Respiratory quinones are predicted by genomics to be of the naphthoquinone type. By genomics, cells are predicted to be able to assimilate sulfate, but unable to grow lithotrophically via the oxidation of either H₂, ammonia, nitrite, or reduced sulfur substrates, or to grow anaerobically via denitrification or dissimilatory nitrate reduction. Based on phylogenetic reconstructions using 16S rRNA gene and/or protein sequences, the genus affiliates within the proposed phylum *Nitrospirota* (*Nitrospirae*), is distinct from the genera comprising the classes *Nitrospira* and *Leptospirillia*, and clusters with sequences from not yet cultivated organisms typically recovered from subsurface karst environments, such as that of “*Ca. Trogloloea absoloni*”.

The type (meta)genome gene sequence for the candidatus species is: DDBJ/ENA/GenBank VTOW00000000^{TS} (DOE-JGI Integrated Microbial Genome ID 2784132095^{TS}); the 16S rRNA gene sequence is GenBank MN381734^{TS}. These were obtained from a two species co-culture along with a putative new species representing the betaproteobacterial genus *Ramlibacter* (Genome sequence: DDBJ/ENA/GenBank VTOX00000000 and DOE-JGI Integrated Microbial Genome ID 2778260901; Genbank 16S rRNA MN381735). The culture was refined from a mixed enrichment culture initiated with manganese carbonate and ca. 250 ml of unsterilized Pasadena (California, USA) municipal drinking water distributed from a tap located on the second floor of the North Mudd Laboratories at the California Institute of Technology (34°08'12.1"N 118°07'38.3"W). The (meta)genome of the type (resolved from the *Ramlibacter* species) is 5.17 Mbp in size, and has a G+C content of 56.4 mol%.

[*Classis* ‘*Ca. Troglolia*’ is represented by “*Ca. Trogloloea absoloni*”; while ‘*Ca. Manganitrophaceae*’, fam. nov., and ‘*Ca. Manganitrophales*’, ord. nov. are typified by “*Ca. Manganitrophus*” and the type (meta)genome sequence DDBJ/ENA/GenBank VTOW00000000^{TS}].

Description of *Ramlibacter lithotrophicus*, sp. nov.

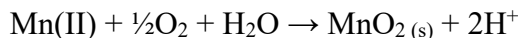
Ramlibacter lithotrophicus (li.tho.tro'phi.cus). Gr. n. lithos stone; N.L. masc. adj. trophicus (from Gr. adj. trophikos), feeding; N.L. masc. adj. lithotrophicus, a capacity for lithotrophic metabolism. Cells exhibit aerobic heterotrophic growth on succinate or tryptone; anaerobic heterotrophic growth with nitrate as electron acceptor; and aerobic chemolithotrophic growth on H₂. Cells are pleomorphic, forming short rods, ca. 1.22 μm by 0.56 μm in dimension, with single, central phase bright inclusions at low cell densities; and fabric-like networks of long filaments of varying width at high cell densities. Cells exhibit twitching surface motility. Colonies are small and featureless on succinate agar defined media or reddish brown on tryptone agar defined media incubated aerobically, and become leathery and adherent upon aging; colonies are red when grown anaerobically with nitrate. By genomics, cells are predicted to be capable of twitching and flagellar motility and to encode putative hydrogenases; putative *sox* and *dsr*MKJOP gene clusters for the lithotrophic oxidation of reduced sulfur compounds; genes for denitrification; and genes for a putative Calvin Cycle. Anaerobic metabolism of aromatic compounds by the tungsten-dependent benzoyl-CoA reductase pathway is predicted by genomics, as is acyl-homoserine lactone based quorum sensing via LuxR and LuxI homologs. Growth has been observed to occur at a pH ranging between 5.7 and 7.4, and at temperatures ranging from 20°C to 40°C. Based on phylogenetic reconstructions using 16S rRNA gene and/or protein sequences, the species affiliates within the betaproteobacterial genus *Ramlibacter*, but is distinct in both gene content and in pairwise similarities from other *Ramlibacter* species.

The type strain for the species is strain RBP-1^T; the genome sequence for the type species is: DDBJ/ENA/GenBank VTOX00000000^{TS} and at DOE-JGI Integrated Microbial Genome ID 2778260901^{TS}; the 16S rRNA gene sequence is GenBank MN381735^{TS}. The strain was isolated on succinate minimal agar media from a two species culture (the other organism being “*Ca. Manganitrophus noduliformans*”) refined from a mixed culture enriched using manganese carbonate and ca. 250 ml of unsterilized Pasadena (California, USA) municipal drinking water that had been distributed from a tap located on the second floor of the North Mudd Laboratories at the California Institute of Technology (34°08'12.1"N 118°07'38.3"W). The genome of the type is 5.26 Mbp in size, and has a G+C content of 69.03 mol%.

Supplementary Notes

Supplementary Note 1: Thermodynamic calculation of Mn(II) oxidation

The Gibbs free energy change of Mn(II) oxidation at pH 7 ($\Delta G^{\circ\prime}$) of the following reaction is determined to be -68 kJ/mol Mn(II) using the standard Gibbs free energy of formation¹⁰⁵:



Values used are: G°_f of Mn(II) = -228 kJ/mol, G°_f of δ -MnO₂ = -453.1 kJ/mol, G°_f of O_{2(g)} = 0 kJ/mol, G°_f of H⁺ = 0 kJ/mol, G°_f of H₂O (l) = -237.18 kJ/mol. The reaction is under standard condition except [H⁺] = 10⁻⁷ M. Note that the composition of birnessite (δ -MnO₂) is not well defined and could range from MnO_{1.74} to MnO_{1.99}¹⁰⁶. The Gibbs free energy change of Mn(II) oxidation could be -80 kJ/mol Mn(II), if G°_f of β -MnO₂ (pyrolusite, the most defined and stable form) = -465.1 kJ/mol were used.

The Nernst equation was used to calculate the reduction potential at pH 7 ($E^{\circ\prime}$) of MnO₂/Mn(II), based on $\Delta G^{\circ\prime}$ of δ -MnO₂ from above and $E^{\circ\prime}$ of O₂/H₂O as +818 mV⁴³, to be +466 mV.

Supplementary Note 2: Growth of Species B

While Species B could be isolated from the Mn(II)-oxidising consortia heterotrophically, its growth varies on different carbon sources tested. On agar plates, Species B grows modestly well with succinate and tryptone, poorly with acetate, and weakly with yeast extract. In liquid cultures, Species B grows well with tryptone with doubling time of 2.89 ± 0.03 hr (n=3, Extended Data Fig. 6c), but poorly with acetate (n=2, Extended Data Fig. 6d), succinate and yeast extract. Species B also grows in liquid cultures lithoautotrophically with hydrogen as the energy source without any organic carbon addition in the medium.

Supplementary Note 3: Evaluation of FISH oligonucleotide probes for Species A and Species B

Three oligonucleotide probes, two newly designed (NLT499, targeting most members of the phylum *Nitrospirae* (*Nitrospirota*) to the exclusion of *Nitrospira*, and BET867, targeting *Betaproteobacteria*) and one previously designed (BET359 targeting *Betaproteobacteria*), was evaluated using the Clone-FISH method⁶⁷. No significant fluorescence intensity decrease was

found for probes NLT499, BET359 and BET867 up to 45%, 35% and 35% formamide concentrations in the hybridization buffer, respectively (Extended Data Fig. 10a-d). No cross-reaction was found when the two Betaproteobacterial probes were applied to 16S rRNA gene clone of Species A (Extended Data Fig. 10a,b), and vice versa when NLT499 probe was applied to 16S rRNA gene clone of Species B (Extended Data Fig. 10c,d).

Supplementary Note 4: Evaluation of the ICP-MS method to measure oxidised and reduced pools of Mn

The ICP-MS method used in this study measured the Mn concentration in the “acid-soluble fraction” and the “acid-insoluble fraction” similar to a previous study⁶. Mn(II) compounds, including MnCl₂, MnSO₄, MnCO₃, should be soluble or become soluble in acid (0.5 M HCl). On the other hand, Mn(IV) oxides should not be acid soluble but solubilized upon reaction with hydroxylamine. Accordingly, almost all Mn content for the Mn(II) compounds were found in the “acid-soluble fraction”, whereas almost all the Mn content for various preparations of Mn(IV) oxides were found in the “acid-insoluble fraction” (Extended Data Fig. 10e).

Mn(III), which could be the predominant Mn species in the environment^{107,108}, could not be clearly distinguished in our method of analysis. Commercial Mn(III)-containing compounds including Mn₃O₄ and Mn₂O₃ showed partitioning in both the “acid-soluble fraction” and the “acid-insoluble fraction” (Extended Data Fig. 10e). Mn₂O₃, with two Mn(III) per compound, partitioned almost equally in the two fractions. Mn₃O₄, with one Mn(II) and two Mn(III) per compound, partitioned about 20:80 in the acid-soluble:acid-insoluble fractions. It seems based on these two test chemicals, Mn(III) partitioning into the two Mn fractions could not be easily predicted based on the average or individual Mn oxidation states. The structure in which hosts Mn(III) likely also contribute to the partitioning as well. In our experiments, we would not be able to distinguish Mn(III) pools and that of Mn(II) and Mn(IV), if Mn(III) were abundant in our cultures. At the end of our kinetic experiments after which the cultures have reached stationary phase with no further cell growth, part of the total Mn was still measured in the reduced pool (Fig. 2; Extended Data Fig. 2). There could be three explanations to this observation: 1) there was still unoxidised Mn(II) left at the end of the experiment and thus measured in the acid soluble pool; 2) Mn oxide biologically produced react and partition differently than that of Mn(IV) oxides tested, and part of biologically produced Mn oxide solubilized and was measured in the reduced pool; 3) there was Mn(III) in the

Mn oxides at the end of the experiment and thus measured in both the acid-soluble and acid-insoluble pools. These three possibilities need to be addressed in future measurements targeting Mn(III)^{107,108}.

However, since Mn(II) in its various forms can be almost entirely measured in the acid-soluble fraction with little in the acid-insoluble fraction, any increase in the acid-insoluble fraction is an indication of oxidised Mn(II). Therefore, in this paper, we refer to the “acid-soluble fraction” as Mn(II), and the “acid-insoluble fraction” as Mn(II) oxidised representing Mn(III/IV).

Supplementary Note 5: Evaluation of quantitative PCR probes for Species A, Species B and Bacteria

In quantitative PCR analyses, the range of bacterial quantification was $1 \cdot 10^4$ to $1 \cdot 10^8$ copies per reaction tube (Extended Data Fig. 10g), similar to the results reported previously on this set of primer-probe combination⁷⁴. In our assays, the background signal was equivalent to approximately $7.5 \cdot 10^3$ copies per reaction tube, higher than previously reported value of $2.5 \cdot 10^3$ copies per reaction tube⁷⁴. High amplification efficiency (101.1% to 102.5%) was found in the bacterial quantification range. There was no difference when either Species A or Species B 16S rRNA gene was used as the template for amplification (Extended Data Fig. 10g). For specific quantification of Species A and Species B, two probes were designed to use in conjunction with the bacterial assay. The quantification ranges of these new probes were found to be $1 \cdot 10^4$ to $1 \cdot 10^7$ copies and $1 \cdot 10^3$ to $1 \cdot 10^7$ copies per reaction tube for Species A and Species B, respectively (Extended Data Fig. 10h). The amplification efficiencies in these ranges were found to be 91.7% for the Species A probe and 94.6% for the Species B probe. While 16S rRNA gene copies could still be detected above or below the quantification ranges, the amplification efficiencies decreased below 90% and thus not used in our analyses. When templates for Species A and Species B were mixed in the same reaction tube, no interference in the quantification of either species was found with the specific probes. The measured 16S rRNA gene copies of Species A and Species B matched closely to that expected in the template mixtures (Extended Data Fig. 10i,j). Overall, our analyses suggest that the specific probes developed in this study work in conjunction with a previously developed assay to quantify 16S rRNA gene copies of Species A, Species B and all Bacteria simultaneously in a single quantitative PCR reaction.

Supplementary Note 6: Ammonia as the anabolic N source for the co-culture

The performance of cultures provided with nitrate as anabolic N source (Main Text) were compared with those supplied with ammonia. Although Species A should be able to transport and assimilate nitrite, cyanate, urea, and ammonia for anabolic N, genomics predicts that it is incapable of assimilating nitrate (Supplementary Table 4). This predicts a dependency on Species B for N in nitrate media, as the latter encodes multiple pathways for nitrate reduction (Supplementary Table 5). Ammonia might be expected to relieve this dependency, meanwhile serving as a superior anabolic N source for both bacteria, with resultant improvements in growth and Mn(II) oxidation. Curiously, for unexplained reasons this was not the case. Mn(II) oxidation rate is comparable if not faster with nitrate than with ammonia: the oxidation rate doubled initially every 6.3 day (s.d. = 1.0, n=4) and slowed to every 10.9 day (s.d. = 0.3, n=4) with nitrate, and doubled initially every 6.0 day (s.d. = 1.2, n=4) and slowed to every 14.5 day (s.d. = 4.0, n=5) with ammonia (Fig. 2a; Extended Data Fig. 2e-l).

For one of the biological replicates with comparable Mn(II) oxidation rate (1 mM nitrate replicate 1 shown in Fig. 2a, and 1 mM ammonia replicate 5 shown in Extended Data Fig. 2l), qPCR assay was used to measure the growth of Species A and Species B. Cell growth is slower with ammonia, with Species A doubling every 9.7 days and Species B doubling every 11.1 days (Extended Data Fig. 2m), compared to Species A doubling every 6.2 days and Species B doubling every 7.4 days (Main Text; Fig. 2b). This slower cell growth also resulted in lower cell yield of roughly half of that of nitrate (Fig. 2c; Extended Data Fig. 2n). Additional experiments are needed to confirm and better understand the underlying reasons for this influence of N source on the co-culture.

Supplementary Note 7: Oxygen respiration and energy conserving respiratory complexes in Species A

On average, the two Mn(II)-derived electrons are generally considered to be of high potential [Mn(II)/Mn(IV), $E^{\circ'}=+466$ mV; above]. However, the energetics of each of the two sequential one-electron transfers can be impacted by inorganic and organic binding ligands^{22,37}, leading to a degree of uncertainty here. While the entry point for each Mn(II) derived electron into electron transport chains remains uncertain, neither electron likely has sufficient negative reduction potential for the reduction of membrane quinones such as ubiquinone ($E^{\circ'}=+113$ mV⁴³).

Of the respiratory complexes, canonical respiratory Complex I is unlikely to be employed for energy conservation, leaving canonical or alternative Complex III, Complex IV, or cytochrome bd oxidases as possible candidates for generating a proton motive force during Mn(II) chemolithotrophy.

While a single Complex IV (cbb3-type heme-copper oxidase) was identified in Species A genome, it was not well-expressed (24th percentile) and therefore likely not the main oxygen reductase under our experimental conditions. Instead, four unconventional terminal oxidase (TO) complexes, each having cytochrome bd oxidase like (bd-like) proteins, dominated expression (Fig. 3b; Supplementary Table 4). Compared to canonical bd oxidases, bd-like proteins have 9-15 (vs 8-9) predicted transmembrane helices, are phylogenetically distinct (Extended Data Fig. 7a), are missing conserved residues including the known quinone-binding sites³⁸ (Extended Data Fig. 8). Also, the oxygen reduction activity of these bd-like oxidase remains to be biochemically confirmed. The bd-like proteins from the 4 terminal oxidases are not alike, and represent 4 distinct evolutionary subclades (Extended Data Fig. 7b). Similar observations have been reported for nitrite-oxidising *Nitrospira*, which showed high expression of these bd-like oxidases in active cultures^{38,39}. In particular, *Nitrospira moscoviensis*: the high expression of bd-like oxidases and low expression of conventional bd oxidases suggest that the bd-like oxidases are likely used in nitrite oxidation, and the conventional oxidases are used for other low potential electron donors³⁹.

The most highly expressed bd-like terminal oxidase complex in Species A was “TO_1” (99th percentile; Fig. 3b), which is also the highest expressed bd-like oxidase in nitrite-oxidising *N. moscoviensis*³⁹. Like homologous complexes from ammonia- and nitrite-oxidising *Nitrospira* (Extended Data Fig. 7b), TO_1 contains a predicted heme b membrane domain homologous to ethylbenzene dehydrogenase gamma subunit EbdC¹⁰⁹, nitrite oxidoreductase gamma subunit NxrC, and other CISM family membrane attachment subunits^{110,111}. However, CISM subunits with molybdate-binding motifs (e.g. NxrAB) typically accompanying these subunits were not identified in Species A. This suggests that TO_1 may receive electrons from alternative periplasmic carriers, such as ferredoxin or cytochrome c (Fig. 3b), perhaps avoiding energy loss associated with electron transfer through the quinone. Energy maybe conserved in the same manner as conventional bd oxidases, which have two proton transfer pathways to generate a proton motive force through scalar reactions without proton pumping¹⁰². The second highest expressed terminal oxidase (TO_2; 83rd percentile; Fig. 3b) also contains a bd-like protein and a membrane-bound, single heme b

EbdC/NxrC homolog, but is otherwise highly unusual amongst cultivated organisms [currently can only be found in an ammonia-oxidizing *Nitrospira* sp. RCA¹¹² and 3 other MAGs in clade IIIb (Extended Data Fig. 7b)]. The c-terminus of the bd-like protein of this complex has two unusual heme c binding sites, and the co-transcribed gene cluster encodes for a split version of the membrane cytochrome b of a conventional Complex III (or cytochrome bf complex), multiple cytochromes c with 1-4 predicted heme c binding sites, and two H⁺/Na⁺ antiporter MrpD-like subunits (Supplementary Table 4). MrpD subunits are homologous to the proton pumping subunits of Complex I (NuoL/M/N) and various hydrogenases (e.g. CooM, HyfB/D/F, EchA)¹¹³. The presence of motive-force generating subunits in a terminal oxidase is unprecedented. Perhaps, complex TO_2 mediates a process similar to that of electron bifurcation in anaerobic archaea and bacteria¹¹⁴, e.g. periplasmic carriers of Mn(II) derived electrons ($E^{\circ'}=+466$ mV) might couple the thermodynamically favourable reduction of O₂ ($E^{\circ'}=+818$ mV)⁴³ to unfavourable Q reduction ($E^{\circ'}\sim+113$ mV) (Fig. 3b). The bd-like proteins of the third (TO_3) and fourth (TO_4) highest expressed terminal oxidase complexes (52nd and 35th percentile, respectively; Fig. 3b) are unusually truncated and occur in each complex as pairs (Extended Data Fig. 7b). Both TO_3 and TO_4 share some resemblance to canonical Complex III and Alternative Complex III^{115,116}, and therefore are predicted to have quinone interactions (Fig. 3b). Their expression suggests that they are not the main terminal oxidases, rather may interact with complexes that generate reduced quinones, such as TO_2.

Supplementary Note 8: Electron balance between catabolism and anabolism in Species A

The biomass yield of Species A is estimated to be 100 mg dry biomass · (mol Mn(II) oxidised)⁻¹, based on DNA yield of 3.1 · 10⁶ ng DNA · (mol Mn(II) oxidised)⁻¹ (Extended Data Fig. 2d), and 3.1% of dry weight of *Escherichia coli* is DNA²⁷. Assuming [CH₂O] as a simplified composition estimate for biomass (30 g dry weight per mol), and given 4 mol electrons needed to reduce 1 mol of CO₂ to 1 mol of [CH₂O], then approximately 0.013 mol of electrons are in the biomass per mol Mn(II) oxidised. With 2 electrons from the Mn(II) oxidation to Mn(IV)O₂, approximately 0.7% of the electrons from Mn(II) oxidation could be recovered in the biomass.

Supplementary Note 9: Stable isotope probing and nanoSIMS analysis

Mn(II)-dependent CO₂ fixation was examined directly in a closed system, using stable isotope probing with Mn¹³CO₃ as the sole source of energy and carbon, after oxidation and growth by cultures that had been initiated with a 10% inoculum from an unlabelled culture. If cells in the culture had engaged in carbon fixation during Mn(II) oxidation, the ¹³C-dissolved inorganic carbon released from the substrate would be the source of label incorporated into the biomass. Before examining for such, the extent of Mn residuum remaining in the samples was examined by nanoSIMS. This was done in order to assess the effectiveness of the Mn oxide nodule dissolution procedure on a fine scale, and to rule out any colocalization of Mn with ¹³C that would indicate that unreacted Mn¹³CO₃ remained in the analysed samples. If associated with cells, unreacted Mn¹³CO₃ would conflict with any proper interpretation on the analysis of the composition of the biomass, but none was observed (Extended Data Fig. 9v).

Because of the high ¹³C amount in our labelled sample, to better resolve the ¹⁵N¹²C secondary ion from that of the ¹⁴N¹³C (both having mass 27): ¹³C¹²C and ¹²C¹²C secondary ions were measured instead ¹³C and ¹²C ions for the carbon stable isotopes. Since there are two possible combinations to obtain ¹³C¹²C ion of mass 25, ²⁵R is twice of ¹³R based on probability (P):

$${}^{25}\text{R} = \frac{{}^{13}\text{C}^{12}\text{C}}{{}^{12}\text{C}^{12}\text{C}} = \frac{P({}^{13}\text{C}) \cdot P({}^{12}\text{C}) + P({}^{12}\text{C}) \cdot P({}^{13}\text{C})}{P({}^{12}\text{C}) \cdot P({}^{12}\text{C})} = \frac{2 \cdot P({}^{13}\text{C})}{P({}^{12}\text{C})} = 2 \cdot {}^{13}\text{R}$$

Carbon isotope was calculated as follows:

$${}^{13}\text{R} = {}^{13}\text{C}/{}^{12}\text{C} = {}^{25}\text{R}/2$$

$${}^{13}\text{F} = {}^{13}\text{C}/({}^{12}\text{C}+{}^{13}\text{C}) = {}^{13}\text{R}/(1+{}^{13}\text{R})$$

$$\text{Atom percent } {}^{13}\text{C} = {}^{13}\text{F} \cdot 100$$

Secondary ions ¹⁴N¹²C and ¹⁵N¹²C were measured on the nanoSIMS for nitrogen stable isotopes ¹⁴N and ¹⁵N respectively.

Nitrogen isotope was calculated as follows:

$${}^{15}\text{R} = {}^{15}\text{N}/{}^{14}\text{N} = {}^{15}\text{N}^{12}\text{C}/{}^{14}\text{N}^{12}\text{C}$$

$${}^{15}\text{F} = {}^{15}\text{N}/({}^{14}\text{N}+{}^{15}\text{N}) = {}^{15}\text{N}^{12}\text{C}/({}^{14}\text{N}^{12}\text{C}+{}^{15}\text{N}^{12}\text{C}) = {}^{15}\text{R}/(1+{}^{15}\text{R})$$

$$\text{Atom percent } {}^{15}\text{N} = {}^{15}\text{F} \cdot 100$$

The application of nanoSIMS revealed that both species fixed $\text{Mn}^{13}\text{CO}_3$ -derived inorganic carbon into cell material. In cell preparations hybridized with species specific fluorescent oligonucleotides, the ^{13}C atom percent in $\text{Mn}^{13}\text{CO}_3$ -grown biomass was determined to be 35.57% (s.d=9.57, n=107) and 7.93% (s.d=5.62, n=27) for cells of Species A and Species B, respectively. These values are strikingly higher than that of ^{13}C natural abundance. Cells grown under the same conditions, but with MnCO_3 synthesized with unlabelled inorganic carbon, were of ^{13}C natural abundance as expected (Extended Data Fig. 9a). Moreover, these values almost certainly underestimate of the full extent of incorporation of inorganic C by both organisms (see discussion on reagents, below). Taking into account the higher ^{13}C atom percent and the markedly higher abundance of Species A cells in the co-culture (Extended Data Fig. 3a), the results indicate that the bulk of the labelled chemosynthate is associated with, and can be attributed to, the activities of Species A.

To better track the synthesis of new biomass, the incorporation of ^{15}N -nitrate and its colocalization with ^{13}C was also examined (and contrasted with the co-localization of Mn and ^{13}C , above) during stable isotope probing analyses. The ^{15}N atom percent in cells were determined to be 57.59% (s.d=8.20, n=107) and 15.77% (s.d=13.30, n=27) for Species A and Species B, respectively (Extended Data Fig. 9a). These results are also consistent with Species A having generated the bulk of the new biomass in the co-culture, given its higher ^{15}N atom percent (Extended Data Fig. 9a) and higher cell abundance (Extended Data Fig. 3a). Such results are not inconsistent with Species A having reductively assimilated the nitrate into its cell material. Yet genomes predict interspecies N crossfeeding from Species B to Species A when growing with nitrate: Species A lacks a recognisable pathway for assimilatory nitrate reduction (Supplementary Table 4), whereas Species B is predicted to be capable of both assimilating and dissimilating nitrate (Supplementary Table 5). Inspection of the FISH coupled nanoSIMS $^{12}\text{C}^{14}\text{N}$ ion image revealed that while Species B cells can have higher ^{14}N contents, Species A cells have higher ^{15}N and a greater ratio of $^{15}\text{N}/^{14}\text{N}$ (Extended Data Fig. 9b-u; Fig. 4). This indicates that either Species B reduces nitrate and shares much of the reduced nitrogen with Species A without incorporating to the same degree itself, or that Species A encodes an unrecognised enzyme for assimilatory nitrate reduction. It is worthnoting that *Nitrospira inopinata*, a relative of Species A in the phylum *Nitrospirae*, does not assimilate either nitrate or nitrite⁹. In any event, the nanoSIMS results confirms that nitrate can serve as the N source for both species in the co-culture, but the

interspecies interaction and effect of ammonia (Supplementary Note 6 above) on the co-culture remain mysterious.

Different preparation methods for samples of cells prior to nanoSIMS analyses can often dilute the stable isotope labels in the biomass, resulting in an underestimate of the actual amounts of ^{13}C and ^{15}N that had been incorporated¹¹⁷. We therefore also performed nanoSIMS analyses on cells without paraformaldehyde fixation and FISH. The resulting atom percent for ^{13}C and ^{15}N in Species A cells increased to 56.56% (s.d=6.51, n=394) and 69.01% (s.d=6.34, n=394), respectively (Extended Data Fig. 9a). There are, however, two main steps in nanoSIMS sample preparation that remain that could dilute the stable isotope label: 1) the dissolution procedure employed to obtain cells from the Mn oxide nodules contained unlabelled reagents (0.05 M sodium dithionite, 0.1 M sodium citrate, 0.1 M sodium bicarbonate and 0.1 M EDTA), and 2) the DAPI-citifluor staining and localization of cells prior to nanoSIMS analysis. Both procedures can dilute the ^{13}C isotopic label in the biomass, thus even these ^{13}C and ^{15}N atom percent values (Extended Data Fig. 9a) likely remain as underestimates of the actual degree of authentic label incorporation that had occurred.

It is not possible from these analyses to ascertain whether or not absolutely 100% of all biomass carbon in the co-culture is derived from CO_2 , and thus chemosynthetic in nature. However, such a degree of incorporation is not necessary to conform to one existing definition of autotrophy⁸, i.e. that a majority of cell carbon is derived from CO_2 -fixation. In such a context and in combination with other evidence, including the composition of the cultivation medium and the expressed CO_2 -fixation pathway genes (Main Text and below), we propose that Species A is operating as a chemolithoautotroph in the manganese-oxidising co-culture.

Supplementary Note 10: Carbon assimilation pathways in Species A

All components in the reverse tricarboxylic acid (rTCA) cycle to produce acetyl-CoA from 2 CO_2 were identified in the Species A genome (Fig. 3b; Supplementary Table 4), except for one of the subunits of fumarate reductase. The fumarate reductase of Species A conforms to the Type E quinone:fumarate oxidoreductases, which contain a catalytic flavoprotein subunit A (SdhA) and an iron-sulfur subunit B (SdhB), but here the canonical membrane subunits C and D (SdhC/D) have been replaced by non-homologous subunits E and F (SdhE/F)¹¹⁸. SdhE with a duplicated motif rich in cysteines CX31-35CCGX38-39CX2C, homologous to heterodisulfide reductase

subunit B, was found in Species A as well as other species in the phylum including *Nitrospira* and *Leptospirillum*^{38,41,119}. However, the small membrane anchor (SdhF) that is thought to link the protein complex to the cell membrane is missing in Species A and its relatives in the phylum, as has been noted previously^{38,41}. The genes in the rTCA cycle of Species A were found to be expressed, including the oft cited key genes for ATP-citrate lyase, oxoglutarate:ferredoxin oxidoreductase (of the O₂ tolerant form with 5 subunits) and fumarate reductase⁴² (Supplementary Table 4). Carbon assimilation from pyruvate is thought to proceed via the Embden-Meyerhof-Parnas (EMP) pathway in *Nitrospira* and *Leptospirillum*^{38,41,119}. However, one of the key genes for the EMP pathway that is found in the related genomes, Class I fructose-bisphosphate aldolase, was not found in the Species A genome. This may or may not be due to any incompleteness in the genome assembly. A homolog of Class II fructose-bisphosphate aldolase (IMG gene ID 2784403887) was found in Species A, but sequence comparisons with characterized class II fructose/tagatose aldolases reveal significant differences, thus whether its substrate is fructose or not remains unclear. In principle, synthesis of hexose sugars from pyruvate can proceed through the Entner-Doudoroff (ED) pathway; however, Species A is missing a recognisable key gene for 6-phosphogluconate dehydratase. A dihydroxy-acid dehydratase¹⁰¹ homolog of 6-phosphogluconate dehydratase can be identified in the Species A genome (IMG gene ID 2784405073), but a phylogenetic analysis building on that of a previous study¹⁰¹ suggest that it is not a good candidate for encoding missing ED pathway enzyme (Extended Data Fig. 5d). Thus from genomics, it is not entirely clear how the biosynthesis of hexoses from pyruvate proceeds in Species A.

In addition to the rTCA cycle, functions of relevance to a partial oxidative TCA (oTCA) cycle could also be identified in Species A, including citrate synthetase, pyruvate carboxylase, and pyruvate dehydrogenase (Fig. 3b; Supplementary Table 4). The only exception in the oTCA cycle not found in Species A is the 2-oxoglutarate dehydrogenase (OGDH) complex, which belongs to the protein family of 2-oxo acid dehydrogenase complexes¹²⁰. All known E1 component of OGDHs are homodimers, but all 5 homologs of the E1 component in the Species A genome were heterotetrameric versions found in pyruvate dehydrogenase and branched-chain 2-oxo acid dehydrogenase complexes but not OGDH complexes¹²⁰. No OGDH with homodimeric versions of the E1 component were identified in characterized relatives in the phylum *Nitrospirae* such as *Ca. Nitrospira defluvii*³⁸, or the genomes of *Nitrospira inopinata* and *Nitrospira moscoviensis*. The 2-

oxoglutarate:ferredoxin oxidoreductase that typical of rTCA cycle has been hypothesized to substitute for this enzymatic step in oTCA cycle with the production of low-potential ferredoxin rather than NADH³⁸, but this scenario would be energetically challenging, if possible at all, under physiological conditions. A more likely scenario is that the oTCA cycles in Species A and members of the phylum *Nitrospirae* are incomplete, as they are so in many autotrophs and non-respiratory, fermentative bacteria. In that case, a partial oTCA branch is probably only for anabolism to generate key intermediate such as 2-oxoglutarate from pyruvate, rather than for respiration and acetate mineralization. Correspondingly, characterized bacteria in the phylum *Nitrospirae*^{48,121} either cannot grow on organic compounds other than formate as the electron donor, or they are incomplete oxidisers¹²² producing acetate rather than CO₂.

Of genes of the EMP, rTCA, and oTCA pathways that were identified, all were expressed. Of the carbon metabolic genes, the most highly expressed in Species A were aconitate hydratase, ATP-citrate lyase and the genes for the three complexes catalyzing CO₂ fixation steps (2-oxoglutarate:ferredoxin oxidoreductase, isocitrate dehydrogenase and pyruvate:ferredoxin oxidoreductase; Fig. 3b). Thus, gene expression under the Mn(II)-oxidation-dependent growth conditions is consistent with CO₂ fixation via the rTCA cycle.

Supplementary Note 11: Unrestricted manganese oxidation calculation

The world manganese ore reserve is estimated to be 630 million metric tonnes¹²³. Starting with a single cell each of Species A and B, and using the estimated doubling time of 6.1 days for Species A (Fig. 2b) and Mn(II) oxidation rate of $1.188 \cdot 10^{-11}$ g substrate·cell⁻¹·day⁻¹ (converted from $9.0 \cdot 10^{-15}$ mol substrate·cell⁻¹·hr⁻¹, Extended Data Fig. 3g), the time (t) needed to generate MnO₂ equalling global Mn reserves with unrestricted chemolithotrophic growth could be estimated by the equation below, which would be within 2 years:

$$Mn(II) \text{ oxidised} = \int_0^t N_0 \cdot k \cdot 2^{\tau/g} d\tau$$

where,

N_0 = starting cell number

t = time needed

k = Mn(II) oxidation rate

g = doubling time

Supplementary Information References

(continue numbering from the main text and methods)

105. Stumm, W. & Morgan, J. J. *Aquatic Chemistry: Chemical Equilibria and Rates in Natural Waters*. (John Wiley & Sons, 2012).
106. Bricker, O. Some stability relations in the system Mn-O₂-H₂O at 25° and one atmosphere total pressure. *Am. Mineral.* **50**, 1296–1354 (1965).
107. Trouwborst, R. E., Clement, B. G., Tebo, B. M., Glazer, B. T. & Luther, G. W. Soluble Mn(III) in suboxic zones. *Science* **313**, 1955–1957 (2006).
108. Madison, A. S., Tebo, B. M., Mucci, A., Sundby, B. & Luther, G. W. Abundant porewater Mn(III) is a major component of the sedimentary redox system. *Science* **341**, 875–878 (2013).
109. Kloer, D. P., Hagel, C., Heider, J. & Schulz, G. E. Crystal structure of ethylbenzene dehydrogenase from *Aromatoleum aromaticum*. *Structure* **14**, 1377–1388 (2006).
110. Rothery, R. A., Workun, G. J. & Weiner, J. H. The prokaryotic complex iron–sulfur molybdoenzyme family. *Biochim. Biophys. Acta BBA - Biomembr.* **1778**, 1897–1929 (2008).
111. Grimaldi, S., Schoepp-Cothenet, B., Ceccaldi, P., Guigliarelli, B. & Magalon, A. The prokaryotic Mo/W-bisPGD enzymes family: A catalytic workhorse in bioenergetic. *Biochim. Biophys. Acta BBA - Bioenerg.* **1827**, 1048–1085 (2013).
112. Poghosyan, L. *et al.* Metagenomic recovery of two distinct comammox *Nitrospira* from the terrestrial subsurface. *Environ. Microbiol.* **21**, 3627–3637 (2019).
113. Moparthi, V. K. *et al.* Functional role of the MrpA- and MrpD-homologous protein subunits in enzyme complexes evolutionary related to respiratory chain complex I. *Biochim. Biophys. Acta BBA - Bioenerg.* **1837**, 178–185 (2014).
114. Buckel, W. & Thauer, R. K. Flavin-based electron bifurcation, ferredoxin, flavodoxin, and anaerobic respiration with protons (Ech) or NAD⁺ (Rnf) as electron acceptors: a historical review. *Front. Microbiol.* **9**, 3704 (2018).
115. Sun, C. *et al.* Structure of the alternative complex III in a supercomplex with cytochrome oxidase. *Nature* **557**, 123–126 (2018).
116. Sousa, J. S. *et al.* Structural basis for energy transduction by respiratory alternative complex III. *Nat. Commun.* **9**, 1728 (2018).
117. Musat, N. *et al.* The effect of FISH and CARD-FISH on the isotopic composition of ¹³C- and ¹⁵N-labeled *Pseudomonas putida* cells measured by nanoSIMS. *Syst. Appl. Microbiol.* **37**, 267–276 (2014).
118. Lemos, R. S., Fernandes, A. S., Pereira, M. M., Gomes, C. M. & Teixeira, M. Quinol:fumarate oxidoreductases and succinate:quinone oxidoreductases: phylogenetic relationships, metal centres and membrane attachment. *Biochim. Biophys. Acta BBA - Bioenerg.* **1553**, 158–170 (2002).
119. Ushiki, N. *et al.* Genomic analysis of two phylogenetically distinct *Nitrospira* species reveals their genomic plasticity and functional diversity. *Front. Microbiol.* **8**, 2637 (2017).
120. Frank, R. A. W., Price, A. J., Northrop, F. D., Perham, R. N. & Luisi, B. F. Crystal structure of the E1 component of the *Escherichia coli* 2-oxoglutarate dehydrogenase multienzyme complex. *J. Mol. Biol.* **368**, 639–651 (2007).
121. Koch, H. *et al.* Expanded metabolic versatility of ubiquitous nitrite-oxidizing bacteria from the genus *Nitrospira*. *Proc. Natl. Acad. Sci. U. S. A.* **112**, 11371–11376 (2015).

122. Frank, Y. A. *et al.* Characterization and genome analysis of the first facultatively alkaliphilic *Thermodesulfovibrio* isolated from the deep terrestrial subsurface. *Front. Microbiol.* **7**, (2016).
123. Cannon, W. F., Kimball, B. E. & Corathers, L. A. *Manganese*. *Manganese* vols 1802–L40 <http://pubs.er.usgs.gov/publication/pp1802L> (2017).